Equilibrium current vortices in simple metals doped with rare earths

Adam B. Cahaya ,[1] Alejandro O. Leon ,[2] Mojtaba Rahimi Aliabad ,[3] and Gerrit E. W. Bauer [4,5,6]

[1]*Department of Physics, Faculty of Mathematics and Natural Sciences, Universitas Indonesia, Depok 16424, Indonesia*
[2]*Departamento de Física, Facultad de Ciencias Naturales, Matemática y del Medio Ambiente, Universidad Tecnológica Metropolitana, Las Palmeras 3360, Ñuñoa 780-0003, Santiago, Chile*
[3]*Nano-Structured Coatings Institute of Yazd Payame Noor University, P.O. Code 89431-74559, Yazd, Iran*
[4]*WPI-AIMR & CSRN, Tohoku University, Sendai 980-8577, Japan*
[5]*Institute for Materials Research, Tohoku University, Sendai 980-8577, Japan*
[6]*The Zernike Institute for Advanced Materials, University of Groningen, Nijenborgh 4, 9747 AG, Groningen, The Netherlands*

Dilute alloys of rare earths have played a vital role in understanding magnetic phenomena. Here, we model the ground state of dilute $4f$ rare-earth impurities in light metals. When the $4f$ subshells are open (but not half-filled), the spin-orbit coupling imprints a rotational charge current of conduction electrons around rare-earth atoms. The sign and amplitude of the current oscillate similar to the Ruderman-Kittel-Kasuya-Yosida (RKKY) spin polarization. We compute the observable effect, namely, the Ørsted field generated by the current vortices and the Knight shift.

I. INTRODUCTION

The conversion of spin currents into excitations of the charge, phonon, photon, or magnetization degrees of freedom and vice versa [1] often involves spin-orbit interactions (SOI) [2]. Examples are the spin-orbit torques [3], charge pumping [4], magnetoelastic interactions [5], and electric-field-induced magnetization dynamics [6,7]. The large intra-atomic SOI that governs the local moments of lanthanides with partially filled $4f$ subshells causes novel spin charge coupling [8] and affects device parameters such as the magnetic damping [9,10]. Rare-earth (RE) ions with local magnetic moments can partially or entirely substitute the nonmagnetic yttrium in the ferrimagnetic insulator yttrium iron garnet $Y_3Fe_5O_{12}$ (YIG) [11]. The different magnetic sublattices of RE-IG strongly modify the magnetic properties [12–14], causing, for example, different compensation points for the magnetic and total angular moments [15]. A more complex phenomenon is a double sign change of the spin Seebeck effect [16]. Thulium iron garnet $(Tm_3Fe_5O_{12})$ films with perpendicular magnetization [17–19] can be switched by current-induced spin-orbit torques [20–22].

These new developments come on top of decades of research on $4f$ electrons in bulk metals [23]. For example, RE impurities in nonmagnetic metals cause an anomalous Hall effect at low doping concentrations [24]. The magnetization in rare-earth intermetallics originates from both the $5d$ and $6s$ conduction electrons and $4f$ moments (see Ref. [25] and references therein). The hybridization of RE moments with conduction electrons affects the susceptibility in rare-earth dialuminides, $REAl_2$ [26], or causes enhanced magnetic moments of RE dopants in Ag and Au [27].

In topological superconductors, such as the Fe(Te, Se), a vortex with a Friedel-like oscillatory profile around magnetic impurities has been reported [28].

Here we present a theoretical study of the coupling of a $4f$ local moment with the Fermi sea of a simple metal host. We predict a charge current circling the impurity with a direction that oscillates radially, as illustrated in Fig. 1. Our starting point for the interaction between the local $4f$ moments and the conduction electrons is the Kondo Hamiltonian [29]. Its chirality induces a circulating current whose vorticity is governed by the direction of the RE orbital moment and generates an Øersted magnetic field. The induced radial current distribution oscillates with the same period as the Ruderman-Kittel-Kasuya-Yosida (RKKY) spin polarization [30] and for the same physical reason, i.e., the finite momentum cutoff at the Fermi surface. The predicted trends should be observable in principle by NMR or scanning microscopy. The present study of the interaction between conduction electrons and $4f$ magnetic moments contributes to understanding spintronic devices, including rare-earth local moments, such as interfaces between rare-earth iron garnets and nonmagnetic metals.

II. LOCAL MOMENTS IN A METALLIC HOST

Rare-earth atoms generally appear in materials as triply charged cations. Their partially filled $4f$ subshell governs their magnetic properties. The $4f$ electrons only weakly interact with their environment [23,31] due to their small orbital radius and shielding by the more extended and fully occupied $5s$ and $5p$ orbitals. This does not exclude a significant exchange interaction: the conduction electrons of Pt contacts activate the Gd moments in gadolinium gallium garnet (GGG) [32]. The exchange interaction between a local spin with conduction electrons of a metal host generates RKKY spin-density oscillations. Triply charged lanthanide anions have electronic configuration [Xe] $4f^n$, where the number of $4f$ electrons n goes from $n = 0$ for La^{+3} to $n = 14$ for Lu^{+3}.
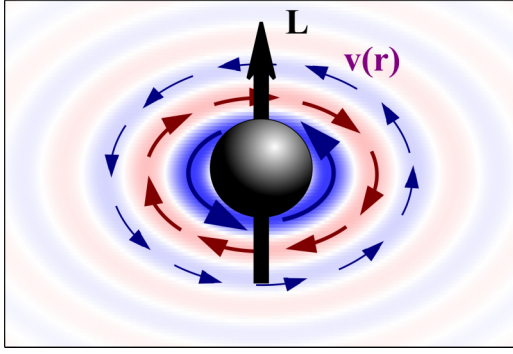
FIG. 1. Schematic representation of the rotational velocity field $\mathbf{v}(\mathbf{r})$ around a rare-earth ion with orbital moment $\mathbf{L}$ embedded in a free-electron gas.

Except for $n = 0$ (La^{+3}), $n = 7$ (Gd^{+3}), and $n = 14$ (Lu^{+3}), the intra-atomic spin-orbit interaction critically affects the magnetic properties. Here we address a spin-orbit proximity effect of such a magnetic moment embedded in a Fermi sea.

A partially occupied $4f$ subshell is characterized by a spin $\mathbf{S}$, an orbital moment $\mathbf{L}$, and a total angular moment $\mathbf{J} = \mathbf{L} + \mathbf{S}$ [23,33]. For the basis $|\Psi\rangle \equiv |S, L, J, J_z\rangle$, $\mathbf{S}^2|\Psi\rangle = \hbar^2 S(S+1)|\Psi\rangle$, $\mathbf{L}^2|\Psi\rangle = \hbar^2 L(L+1)|\Psi\rangle$, $\mathbf{J}^2|\Psi\rangle = \hbar^2 J(J+1)|\Psi\rangle$, $\hat{J}_z|\Psi\rangle = \hbar J_z|\Psi\rangle$, where $\hbar$ is the reduced Planck constant. Hund's rules specify the quantum numbers S, L, and J of the ground-state manifold, while J_z depends on the applied magnetic and electric fields. Within a manifold of constant S, L, and J, the Wigner-Eckart theorem ensures collinearity of all angular moment vectors: $\mathbf{S} = (g_J - 1)\mathbf{J}$, $\mathbf{L} = (2 - g_J)\mathbf{J}$, and $\mathbf{L} + 2\mathbf{S} = g_J\mathbf{J}$, where $g_J = 3/2 + [S(S+1) - L(L+1)]/[2J(J+1)]$ is the Landé g factor.

We model the system as a single RE local moment embedded into a free-electron gas, which is appropriate for most dilute alloys. Conduction electrons interact with the rare-earth spin and orbital moment via the Kondo Hamiltonian [29]. Here we address equilibrium properties that are affected by the spin-independent skew scattering but disregard external current-induced phenomena such as the spin-Hall effect. We operate in a regime above the Kondo temperature and treat $\mathbf{J}$, $\mathbf{S}$, and $\mathbf{L}$ as classical vectors. The strongly localized $4f$ orbital radius governs the spatial extent of the coupling. When the $4f$ orbital radius is much smaller than the typical wavelength of the conduction electrons, the moment couples to free electrons by a contact interaction.

The s-f exchange interaction in the Kondo Hamiltonian is similar to the s-d Hamiltonian for $3d$ transition metals [29,31,34,35]. It reads

$$H_{sf} = -\frac{J_{ex}}{\hbar^2}\delta^{4f}(\mathbf{r})\mathbf{S}\cdot\frac{\hbar\boldsymbol{\sigma}}{2}, \qquad (1)$$

where $\boldsymbol{\sigma}$ is the vector of Pauli matrices, and $\delta^{4f}(\mathbf{r})$ is a Dirac δ representing the localized $4f$ subshell. In a free-electron gas with Fermi wave number k_F, the exchange constant [29] is $J_{ex} = 2e^2 A_3(0)/(7\epsilon_0 k_F^2)$, where the radial integral [29] $A_h(n) = \int_0^\infty dx_1 x_1^2 \int_0^\infty dx_2 x_2^2 j_n(x_1) j_n(x_2) x_<^h/x_>^{h+1} R(r_1) R(r_2)$, with $x_1 = k_F r_1$, $x_2 = k_F r_2$, $x_< = \min(x_1, x_2)$, and $x_> = \max(x_1, x_2)$. $A_h(n)$ can be evaluated numerically

using a Slater-type orbital for the radial part of the $4f$ wave function $R(r) \sim r^3 e^{-r/a}$ normalized over a large volume, $\int_0^\infty dr r^2 R^2(r) = 1$. The constant a is related to the $4f$ radius by $\langle r \rangle = \int_0^\infty dr r^3 R^2(r) = 9a/2$. With $k_F = 1.75$ Å^{-1} for Al and $\langle r \rangle = 0.6$ Å [23], $A_3(0) = 0.33$ and $J_{ex} = 5.6$ eV Å^3.

The so-called spin-*in*dependent skew scattering affects the trajectories of the electron charge and is responsible for the anomalous Hall effect in metals with RE impurities [24,29,36]. As shown below, it also affects the ground state. Its Hamiltonian reads [29]

$$H_{skew} = \mathbf{L}\cdot\left([\nabla\eta(\mathbf{r})]\times\frac{1}{i}\nabla\right)\mathbb{I}_{2\times2}, \qquad (2)$$

where $\mathbb{I}_{2\times2}$ is the identity matrix in Pauli spin space, and $\eta(\mathbf{r}) = \eta_0\delta^{4f}(\mathbf{r})$ with $\eta_0 = 9e^2[A_2(1) - (5/9)A_4(1)](140\epsilon_0\hbar k_F^4)^{-1}$. For the parameters introduced above, $A_2(1) \sim 0.0885$, $A_4(1) = 0.056$, and $\hbar\eta_0 k_F^2 = 0.21$ eV Å^3. Both exchange and skew-scattering interactions are active in a volume $V_{4f} \lesssim 10$ Å^3. The energy scales $\langle H_{skew} \rangle \sim \hbar\eta_0 k_F^2/V_{4f} = \mathcal{O}(10\,\text{meV})$ and $\langle H_{sf} \rangle \sim J_{ex}/V_{4f} = \mathcal{O}(100\,\text{meV})$ are consistent with published values extracted from experiments, such as the Knight shift [37], electron spin resonance [38], and magnetoresistance [39–41]. H_{skew} deflects free electrons via an effective local force caused by the $4f$ subshell with orbital angular momentum $\mathbf{L}$. Equation (2) does not contain an explicit SOI parameter, because we operate in the limit of large $4f$ spin-orbit interaction that generates a finite $|\mathbf{L}|$.

The $4f$ RE impurities in noble metals hybridize with $5d$ virtual bound states of the conduction electrons [42], which can be parameterized in terms of phase shifts of angular momentum scattering channels [40]. The enhancement of the magnetic moments of pure RE metals [43–45] and in RE-doped Ag and Au [27,46] has been attributed to those $5d$ virtual bound states. Here we focus on the spin and orbital polarization induced by the Kondo Hamiltonian on conduction electrons that we describe by plane waves without truncating an expansion into spherical harmonics. To leading order in the contact interaction, we may discard hybridization and orthogonalization corrections.

Next we discuss the RKKY spin polarization due to the H_{sf} and the response induced by H_{skew}. We focus on ions with partially filled $4f$ shells. Gd^{3+} ($L = 0$) can create an RKKY spin polarization, but its H_{skew} vanishes. We do not address Eu^{3+} since its spin and orbital moments cancel in its ground ($J = 0$) but not in excited states.

III. RKKY SPIN-DENSITY OSCILLATIONS

In the mean-field, local-density approximation, Eq. (1) for an RE moment at the origin $\mathbf{r} = 0$ becomes

$$H_{sf} = -\frac{J_{ex}}{\hbar^2}\mathbf{s}(\mathbf{r} = 0)\cdot\mathbf{S}, \qquad (3)$$

where $\mathbf{s}(\mathbf{r}) \equiv \langle\Psi_c^\dagger(\mathbf{r})|\hbar\boldsymbol{\sigma}/2|\Psi_c(\mathbf{r})\rangle$ is the spin density of the conduction-electron wave function Ψ_c. For a static moment
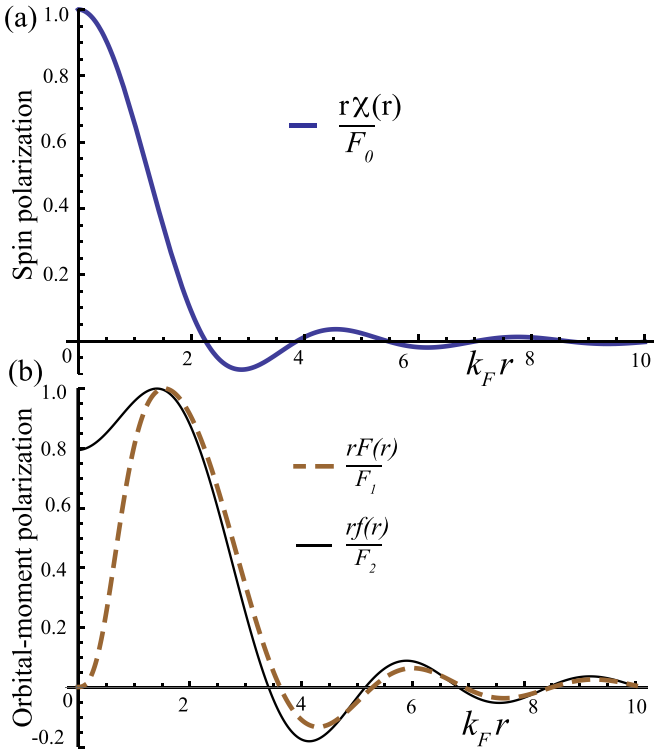
FIG. 2. Distribution of the spin and orbital polarizations close to a RE local moment in the free-electron gas. (a) RKKY spin-density oscillations $r\chi(r)/F_0$ normalized by $F_0 = \lim_{r\to 0} r\chi(r)$. (b) Distribution of the induced orbital moment obtained with the regularized and nonregularized response functions, $rF(r)/F_1$ and $rf(r)/F_2$, respectively, normalized by their maximum values obtained approximately for $k_F r = 3/2$, $F_1 = \max[rF(r)]$, and $F_2 = \max[rf(r)]$. The response is dominantly paramagnetic but oscillates with diamagnetic contributions. Far from the atom, the spin and orbital responses share an oscillating algebraic decay $\cos(2k_F r)/r^3$. As this figure illustrates, the distributions have a phase difference for small radius.

and to leading order in J_{ex}, we recover the RKKY spin-density oscillations

$$\langle \mathbf{s} \rangle (r) = \frac{J_{ex}}{\hbar^2} \chi(r) \mathbf{S}, \tag{4}$$

$$\chi(r) = \frac{D_e \hbar^2}{16\pi r^3} \left[\frac{\sin(2k_F r)}{2k_F r} - \cos(2k_F r) \right], \tag{5}$$

where $\chi(r)$ is the susceptibility and $D_e = m_e k_F (\pi\hbar)^{-2}$ the density of states of the host metal at the Fermi energy. Figure 2(a) illustrates the characteristic RKKY oscillations in $r\chi(r)$ that contribute to the total spin magnetic moment $\mathbf{m}_S$,

$$\mathbf{m}_S = -\gamma_0 g_S \int d^3r [\mathbf{S}\delta(\mathbf{r}) + \langle \mathbf{s} \rangle (\mathbf{r})] = -\gamma_0 g_S (1 + G_i^S) \mathbf{S}, \tag{6}$$

where the bare g factor is $g_S = 2$, $\gamma_0 = e/(2m_e)$ is the modulus of the gyromagnetic ratio, $-e$ is the electron charge, and the constant $G_i^S = J_{ex} D_e/4$. For example, in Al, $G_i^S \approx 0.13$. The polarization cloud enhances the total spin magnetic moment and g factor by G_i^S, which can be observed via the imaginary part of the spin-mixing conductance (effective field) at ferromagnet|normal metal interfaces [47] or spin-dependent

interfacial phase shifts at ferromagnet| superconductor interfaces [48].

IV. ROTATIONAL CURRENTS

We now show that the Kondo Hamiltonian generates equilibrium charge-current vortices around the impurity. In Fourier representation with linear momentum $\hbar\mathbf{q}$ and unperturbed wave function $\langle \mathbf{r}|\mathbf{q}\rangle = e^{i\mathbf{r}\cdot\mathbf{q}}/\sqrt{\Omega}$, the matrix elements of the skew-type interaction read

$$\langle \mathbf{q} + \mathbf{k}|H_{skew}|\mathbf{q}\rangle = i\eta_0 \Omega^{-1} e^{-2k^2 a^2}(\mathbf{k} \times \mathbf{q}) \cdot \mathbf{L}, \tag{7}$$

where $e^{-2k^2 a^2}$ cuts off an ultraviolet divergence of a δ-function potential. To leading order in η_0, we find a spin-independent velocity field of conduction electrons (see Appendix A):

$$\langle \mathbf{v}(\mathbf{r}) \rangle = \frac{\eta_0}{2\pi^3 \hbar} \frac{F(r)}{r} \mathbf{L} \times \hat{\mathbf{r}}, \tag{8}$$

where

$$F(r) = \frac{1}{ar\sqrt{2\pi}} \int_0^\infty \frac{dr'}{r'} e^{-\frac{r'^2 + r^2}{8a^2}} f_1(r, r') f(r'), \tag{9}$$

$$f_1(r, r') = r'r \cosh\left(\frac{r'r}{4a^2}\right) - 4a^2 \sinh\left(\frac{r'r}{4a^2}\right), \tag{10}$$

$$f(x/k_F) = \frac{2x(-9 + 2x^2)\cos(2x) + (9 - 14x^2)\sin(2x)}{8(x/k_F)^6}, \tag{11}$$

and $x = k_F r$. In the δ-function $a \to 0$, the response function f should used in Eq. (8) instead of F. Outside the $4f$ subshell, F and f are similar, see Fig. 2(b). F, f, and χ oscillate with wave number $2k_F$ and are approximated by $\cos(2k_F r)/r^3$ far from the atom. The integrated modulus of the velocity,

$$\bar{v}_s = \int |\langle \mathbf{v} \rangle| d^3r = 0.01 v_F \left(\frac{(2 - g_J)\sqrt{J(J+1)}}{4} \right), \tag{12}$$

is of the order of a percent of the Fermi velocity $v_F = \hbar k_F/m_e \sim 2 \times 10^6$ m/s and $\bar{v}_s \sim 10$ km/s for Al.

The radial density of the orbital angular momentum,

$$\langle \mathbf{l} \rangle (r) \equiv \iint \frac{d\phi d\theta \sin\theta}{4\pi} m_e \mathbf{r} \times \langle \mathbf{v}_s(\mathbf{r}) \rangle = \frac{m_e \eta_0 F(r)}{3\pi^3 \hbar} \mathbf{L}, \tag{13}$$

is at equilibrium always collinear with $\mathbf{L}$ and parallel to it near the origin. Both the orbital density of the rotational current and the RKKY spin polarization decay algebraically and oscillate with increasing distance from the origin [see Fig. 2(b)]. Therefore the current response has paramagnetic as well as diamagnetic contributions. Note that the spin and orbital radial distributions have a phase difference for small radius, as shown in Fig. 2.

The orbital magnetic moment is dressed by the electron gas

$$\mathbf{m}_L = -\gamma_0 g_L \int d^3r [\mathbf{L}\delta(\mathbf{r}) + \langle \mathbf{l} \rangle (\mathbf{r})] = -\gamma_0 g_L (1 + G_i^L) \mathbf{L}, \tag{14}$$

where the bare orbital g-factor $g_L = 1$, and $G_i^L = 2m_e \eta_0 k_F^3/(3\pi^2 \hbar)$, or
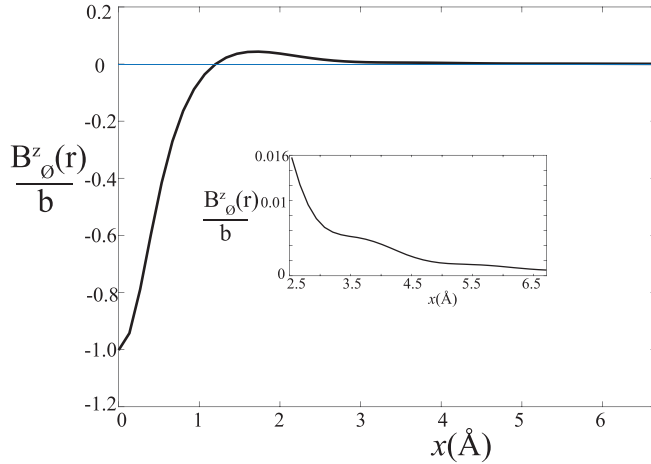
$$G_i^L = n_{4f} \frac{E_\eta}{E_F}, \tag{15}$$

FIG. 3. The z-component of the Ørsted field near a RE atom in the free-electron gas. $B_{\varnothing}^z = \mathbf{e_z} \cdot \mathbf{B}_{\varnothing}$, as a function distance ($\mathbf{r} = x\mathbf{e_x}$), where $\mathbf{e_j}$ is the unit vector along the Cartesian axis j. The field is normalized by its modulus at the origin $b = |\mathbf{B}_{\varnothing}(\mathbf{0})|$.

where $n_{4\mathrm{f}} = V_{4\mathrm{f}} n_0$ is the number of conduction electrons in the volume of the $4f$ subshell, $V_{4\mathrm{f}} \sim 10\,\text{Å}^3$, with $n_0 = k_F^3/(3\pi^2)$ the metal density. The energy of orbital-orbital coupling is $E_\eta = \hbar \eta_0 k_F^2/V_{4\mathrm{f}}$, while the host Fermi energy is $E_F = \hbar^2 k_F^2/(2m_e)$. Thus the strength of the rotational current momentum, with respect to $\mathbf{L}$, is proportional to the ratio of the orbital coupling and Fermi energies. The proportionality constant is the average number of conduction electrons subject to the coupling potential. For the present parameters we find $n_{4\mathrm{f}} \approx 1.8$, $E_\eta \approx 0.02\,\text{eV}$, $E_F = 11.7\,\text{eV}$, and a relatively small value $G_i^L \approx 1/300$.

The current vortex induces an Ørsted field

$$\mathbf{B}_{\varnothing}(\mathbf{r}) = -\frac{e\mu_0}{4\pi} \int d^3 r' \langle \mathbf{v}(\mathbf{r'}) \rangle \times \frac{\mathbf{r} - \mathbf{r'}}{|\mathbf{r} - \mathbf{r'}|^3}, \qquad (16)$$

where $\mu_0 = 4\pi \times 10^{-7}\,\text{J}/(\text{mA}^2)$ is the magnetic permeability of free space. The velocity and magnetic fields are proportional to the RE orbital momentum, $|\langle \mathbf{v} \rangle| \propto |\mathbf{B}_{\varnothing}| \propto \eta_0 |\mathbf{L}|$. Far from the RE ion, $R \gg \langle r \rangle$,

$$\mathbf{B}_{\varnothing}(\mathbf{R}) = \frac{\mu_0}{4\pi} \frac{3(\mathbf{m_{rc}} \cdot \mathbf{R})\mathbf{R} - R^2 \mathbf{m_{rc}}}{R^5} \qquad (17)$$

is the field generated by the magnetic dipole $\mathbf{m_{rc}} = -\gamma_0 G_i^L \mathbf{L}$. $\mathbf{B}_{\varnothing}$ is proportional to the dipolar magnetic field by the $4f$ orbital momentum ($\mathbf{B_L}$), i.e., $\mathbf{B}_{\varnothing} = G_i^L \mathbf{B_L}$, with $G_i^L \ll 1$.

At the origin and for $k_F = 1.75/\text{Å}$,

$$\mathbf{B}_{\varnothing}(\mathbf{0}) = -3.5 \times 10^{-7} e\eta_0 \mu_0 a^{-6}(\mathbf{L}/\hbar),$$

$$= 0.06\,\text{T} \left(\frac{(2 - g_J)\sqrt{J(J+1)}}{4} \right).$$

Figure 3 shows the z component of this field as a function of distance $\mathbf{r} = x\mathbf{e_x}$, where the unit vectors $\mathbf{e_x}$ and $\mathbf{e_z}$ point along the x and z Cartesian axis, respectively. The field is negative close to the origin but turns positive and decays to zero in an oscillatory fashion.

The field at the origin, $\mathbf{B}_{\varnothing}(\mathbf{0})$, couples to the local nuclear spin by the Zeeman interaction, which shifts the NMR
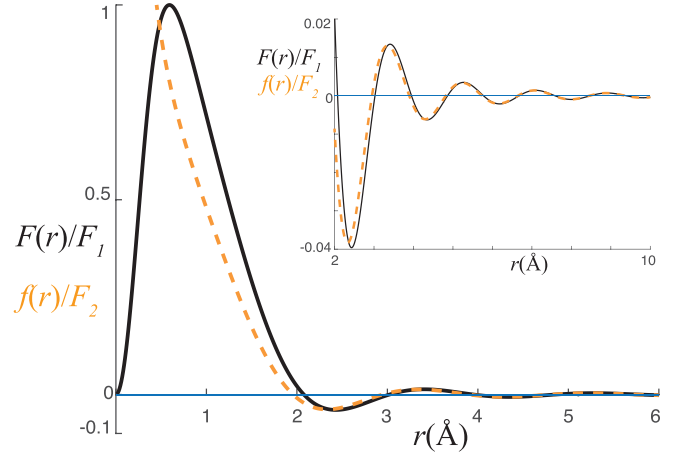

FIG. 4. Response functions $F(r)$ and $f(r)$ that describe the regularized and nonregularized velocities, respectively. They are normalized by the maximum value of $F_1 \equiv \max[F(r)]$ and by $F_2 = F_1 f(r_0)/F(r_0)$, such that they have the same value at the (arbitrarily chosen) point $r_0 = 3.34\,\text{Å}$. The inset shows the behavior of the curves for large distances. As this figure illustrates, the curves have the same feature outside the rare-earth atom. However, only the regularized function f is finite inside the $4f$ subshell.

frequency by $\Delta\omega = \gamma_N |\mathbf{B}_{\varnothing}(\mathbf{0})| \sim 5\,\text{MHz}$, where γ_N is the nuclear gyromagnetic ratio. In NMR experiments, a constant magnetic field $B_0 \mathbf{e_z}$ polarizes the nuclear moments as well as the $4f$ moments along the z direction. The Knight shift K, produced by the current and parameterized by the ratio of the internal and applied magnetic fields [49], at low temperatures ($T \lesssim 1$ K) is

$$K \equiv \frac{|\mathbf{B}_{\varnothing}(0)|}{B_0} = -0.3\% \left(\frac{(2 - g_J)\sqrt{J(J+1)}}{4} \right) \left(\frac{20\,\text{T}}{B_0} \right), \tag{18}$$

where we assume full polarization of the magnetic moment of the $4f$ subshell. The NMR frequency is typically in the 100-MHz regime for applied (constant) fields of $B_0 \sim 10$ T. For a given rf frequency we therefore predict different resonance magnetic fields for rare-earth impurities in an insulating and metallic host. We hope that our results stimulate experiments that can identify the ground-state current vortices.

Orbital contributions to the Knight shift have been predicted before [27,50], holding virtual bound states of conduction electrons at RE impurities in a metal host responsible [27]. These theories are not compatible with our model since they predict effects for half-filled shells without orbital moment (Gd).

V. CONCLUSIONS

We predict that RE local moments interact with the conduction electrons of a metallic host to generate both an oscillating spin density and charge current, the latter by the spin-*in*dependent skew-scattering interaction. The radial distribution of the induced velocity field oscillates with the same period as the RKKY spin polarization induced by the local exchange interaction. A finite $4f$ orbital moment $\mathbf{L}$ is necessary to form the current in the electron gas. Therefore the predicted magnetic field and Knight shift depend linearly with

$|\mathbf{L}| \propto (2 - g_J)|\mathbf{J}|$ and vanish for RE-doped insulators. Furthermore, the induced magnetic field depends on the atomic number via the Landé g factor ground-state quantum numbers. Several approximations are crude, but we are confident about the predicted trends. Relativistic first-principles calculations of open $4f$ subshells in a metal host should improve the accuracy of the predictions.

The Ørsted fields generated by RE impurities at the surface of a metal with sufficiently large Fermi wavelength can be measured in principle by scanning magnetometries based on nanoscale superconducting quantum interference devices (nanoSQUID) [51] or optically read-out nitrogen-vacancy (NV) centers [52,53]. RE impurities adsorbed at a surface two-dimensional electron gas or graphene monolayer are promising candidate systems to image the predicted equilibrium current vortices.

APPENDIX A: ROTATIONAL CURRENTS

Here we derive the linear response of a simple metal to a rare-earth (RE) magnetic impurity characterized by the classical vectors $\mathbf{S}$, $\mathbf{L}$, and $\mathbf{J}$, i.e., the spin, orbital, and total angular momenta, respectively. The conduction-electron orbital angular momentum density $\mathbf{l} = m_e \mathbf{r} \times \mathbf{v}(\mathbf{r})$ relative to the local moment at the origin, where $m_e \mathbf{v}(\mathbf{r})$ is the linear momentum density, reads in second quantization (see also Appendix C)

$$\mathbf{l}(\mathbf{r}) = \hbar \mathbf{r} \times \frac{1}{\Omega} \sum_{\mathbf{p}\mathbf{q}\gamma} e^{i(\mathbf{q}-\mathbf{p})\cdot\mathbf{r}} \frac{\mathbf{p}+\mathbf{q}}{2} a_{\mathbf{p}\gamma}^\dagger a_{\mathbf{q}\gamma}. \quad (A1)$$

We define the expectation values $\langle \mathbf{v} \rangle = \mathrm{Tr}[\rho \mathbf{v}]$, where Tr stands for the trace, and ρ is the density matrix of the full Hamiltonian. With the time-evolution operator in the interaction picture, $U(t) \equiv \exp\left[-(i/\hbar)\int_{t_0}^t H_{\mathrm{skew}}(t')dt'\right]$, the total density matrix ρ can be written in terms of the ground-state density matrix ρ_0 of the unperturbed free-electron gas with Hamiltonian H_0 and the regularized skew-scattering Hamiltonian

$$H_{\mathrm{skew}} = \frac{i\eta_0}{\Omega} \sum_{\mathbf{k}\mathbf{q}'\gamma'} e^{-2k^2 a^2} a_{\mathbf{q}'+\mathbf{k}\ \gamma'}^\dagger a_{\mathbf{q}'\gamma'} (\mathbf{k} \times \mathbf{q}') \cdot \mathbf{L}, \quad (A2)$$

where the constant $a = 2\langle r \rangle / 9$, related to the $4f$ subshell radius $\langle r \rangle \sim 0.6\text{Å}$, accounts for the finite spatial extension of the $4f$ Slater-type orbital $R(r) \propto r^3 e^{-r/a}$. The exponential $e^{-2k^2 a^2}$ cuts off an ultraviolet divergence that would arrive for a δ-function perturbation. For an Al host metal, $\hbar\eta_0 k_F^2 = 0.21$ eV Å^3. Then,

$$\langle \mathbf{v}(\mathbf{r}) \rangle = \mathrm{Tr}[\rho_0 \hat{U}^{-1}(t)\mathbf{v}\hat{U}(t)],$$
$$\approx \mathrm{Tr}\left[\rho_0\left(1 + \frac{i}{\hbar}\int_{-\infty}^t H_{\mathrm{skew}}(t')dt'\right)\mathbf{v}\right.$$

$$\left. \cdot \left(1 - \frac{i}{\hbar}\int_{-\infty}^t H_{\mathrm{skew}}(t')dt'\right)\right],$$
$$= \frac{i}{\hbar}\left\langle \int_{-\infty}^t dt'[H_{\mathrm{skew}}(t'), \mathbf{v}(\mathbf{r})]\right\rangle_0, \quad (A3)$$

where $\langle A \rangle_0 = \mathrm{Tr}[\rho_0 A]$. This leads to

$$\langle \mathbf{v}(\mathbf{r}) \rangle = -\frac{i}{m_e\Omega}\int_{-\infty}^t dt' \sum_{\mathbf{p}\mathbf{q}\gamma} e^{i(\mathbf{q}-\mathbf{p})\cdot\mathbf{r}}\frac{\mathbf{p}+\mathbf{q}}{2}$$

$$\langle [a_{\mathbf{p}\gamma}^\dagger(t)a_{\mathbf{q}\gamma}(t), H_{\mathrm{skew}}\ (t')]\rangle_0$$

$$= \frac{\eta_0}{m_e\Omega^2} \sum_{\mathbf{k}\mathbf{q}'\gamma'} e^{-2k^2 a^2} \sum_{\mathbf{p}\mathbf{q}\gamma} e^{i(\mathbf{q}-\mathbf{p})\cdot\mathbf{r}}\frac{\mathbf{p}+\mathbf{q}}{2}(\mathbf{k} \times \mathbf{q}') \cdot \mathbf{L}$$

$$\int_{-\infty}^t dt' \langle [a_{\mathbf{p}\gamma}^\dagger(t)a_{\mathbf{q}\gamma}(t), a_{\mathbf{q}'+\mathbf{k}\ \gamma'}^\dagger(t')a_{\mathbf{q}'\gamma'}(t')]\rangle_0. \quad (A4)$$

The susceptibility is

$$\chi(t - t') = \Theta(t - t') \sum_{\gamma\gamma'} \langle [a_{\mathbf{p}\gamma}^\dagger(t)a_{\mathbf{q}\gamma}(t),$$
$$a_{\mathbf{q}'+\mathbf{k}\gamma'}^\dagger(t')a_{\mathbf{q}'\gamma'}(t')]\rangle_0, \quad (A5)$$

where Θ is the Heaviside step function with time derivative

$$\partial_t \chi(t - t')$$
$$= \delta(t - t') \sum_{\gamma\gamma'} \langle [a_{\mathbf{p}\gamma}^\dagger(t)a_{\mathbf{q}\gamma}(t), a_{\mathbf{q}'+\mathbf{k}\gamma'}^\dagger(t')a_{\mathbf{q}'\gamma'}(t')]\rangle_0$$
$$+ \Theta(t - t') \sum_{\gamma\gamma'} \langle [\partial_t(a_{\mathbf{p}\gamma}^\dagger(t)a_{\mathbf{q}\gamma}(t)),$$
$$a_{\mathbf{q}'+\mathbf{k}\gamma'}^\dagger(t')a_{\mathbf{q}'\gamma'}(t')]\rangle_0. \quad (A6)$$

$\partial_t[a_{\mathbf{p}\gamma}^\dagger(t)a_{\mathbf{q}\gamma}(t)]$ can be calculated by the Heisenberg equation for the electron gas $H_0 = \sum_{\mathbf{k}\gamma} \epsilon_{\mathbf{k}} a_{\mathbf{k}\gamma}^\dagger a_{\mathbf{k}\gamma}$ with parabolic dispersion relation $\epsilon_{\mathbf{k}} = \hbar^2 \mathbf{k}^2/(2m_e)$,

$$\partial_t(a_{\mathbf{p}\gamma}^\dagger a_{\mathbf{q}\gamma}) = \frac{1}{i\hbar}[a_{\mathbf{p}\gamma}^\dagger a_{\mathbf{q}\gamma}, H_0]$$
$$= \frac{1}{i\hbar}\left[a_{\mathbf{p}\gamma}^\dagger a_{\mathbf{q}\gamma}, \sum_{\mathbf{k}\gamma'} \epsilon_{\mathbf{k}} a_{\mathbf{k}\gamma'}^\dagger a_{\mathbf{k}\gamma'}\right]$$
$$= -\frac{i}{\hbar}(\epsilon_{\mathbf{q}} - \epsilon_{\mathbf{p}})a_{\mathbf{p}\gamma}^\dagger a_{\mathbf{q}\gamma}, \quad (A7)$$

and

$$\sum_{\gamma\gamma'}[a_{\mathbf{p}\gamma}^\dagger a_{\mathbf{q}\gamma}, a_{\mathbf{q}'+\mathbf{k}\gamma'}^\dagger a_{\mathbf{q}'\gamma'}]$$
$$= \sum_{\gamma}(\delta_{\mathbf{q},\mathbf{q}'+\mathbf{k}} a_{\mathbf{p}\gamma}^\dagger a_{\mathbf{q}-\mathbf{k}\gamma} - \delta_{\mathbf{p},\mathbf{q}'} a_{\mathbf{p}+\mathbf{k}\gamma}^\dagger a_{\mathbf{q}\gamma}). \quad (A8)$$

χ then satisfies the equation of motion

$$\left(\partial_t + \frac{i}{\hbar}(\epsilon_{\mathbf{q}} - \epsilon_{\mathbf{p}})\right)\chi(t - t')$$
$$= \delta(t - t')\left\langle \sum_{\gamma}(\delta_{\mathbf{q},\mathbf{q}'+\mathbf{k}} a_{\mathbf{p}\gamma}^\dagger a_{\mathbf{q}-\mathbf{k}\gamma} - \delta_{\mathbf{p},\mathbf{q}'} a_{\mathbf{p}+\mathbf{k}\gamma}^\dagger a_{\mathbf{q}\gamma})\right\rangle_0. \quad (A9)$$

In the frequency domain, with $\chi(t) = (2\pi)^{-1} \int d\omega \chi(\omega) e^{-i\omega t}$,

$$\chi(\omega) = i\hbar \frac{\sum_\gamma \langle \delta_{\mathbf{q},\mathbf{q'}+\mathbf{k}} a^\dagger_{\mathbf{p}\gamma} a_{\mathbf{q}-\mathbf{k}\gamma} - \delta_{\mathbf{p},\mathbf{q'}} a^\dagger_{\mathbf{p}+\mathbf{k}\gamma} a_{\mathbf{q}\gamma} \rangle_0}{\epsilon_\mathbf{p} - \epsilon_\mathbf{q} + \hbar\omega + i0^+}$$

$$= 2i\hbar \frac{\delta_{\mathbf{q},\mathbf{q'}+\mathbf{k}}\delta_{\mathbf{p},\mathbf{q}-\mathbf{k}}f_\mathbf{p} - \delta_{\mathbf{p},\mathbf{q'}}\delta_{\mathbf{q},\mathbf{p}+\mathbf{k}}f_\mathbf{q}}{\epsilon_\mathbf{p} - \epsilon_\mathbf{q} + \hbar\omega + i0^+}, \quad \text{(A10)}$$

where $f_\mathbf{p}$ is the (spin-degenerate) Fermi-Dirac distribution. Substituting χ into Eq. (A4) after transformation into the frequency domain and in the steady state ($\omega \to 0$),

$$\langle \mathbf{v}(\mathbf{r}) \rangle = \frac{\eta_0}{m_e \Omega^2} \sum_{\mathbf{k}\mathbf{q'}} e^{-2k^2 a^2} \sum_{\mathbf{p}\mathbf{q}} e^{i(\mathbf{q}-\mathbf{p})\cdot\mathbf{r}}(\mathbf{p}+\mathbf{q})$$

$$\cdot [(\mathbf{k}\times\mathbf{q'})\cdot\mathbf{L}]i\hbar \frac{\delta_{\mathbf{q},\mathbf{q'}+\mathbf{k}}\delta_{\mathbf{p},\mathbf{q}-\mathbf{k}}f_\mathbf{p} - \delta_{\mathbf{p},\mathbf{q'}}\delta_{\mathbf{q},\mathbf{p}+\mathbf{k}}f_\mathbf{q}}{\epsilon_\mathbf{p} - \epsilon_\mathbf{q} + i0^+}$$

$$= \frac{i\eta_0\hbar}{m_e \Omega^2} \sum_{\mathbf{p}\mathbf{q}} e^{-2a^2|\mathbf{p}-\mathbf{q}|^2} e^{i(\mathbf{q}-\mathbf{p})\cdot\mathbf{r}}(\mathbf{p}+\mathbf{q})$$

$$\left(\mathbf{L} \cdot \frac{-\mathbf{p}\times\mathbf{q}f_\mathbf{p} - \mathbf{q}\times\mathbf{p}f_\mathbf{q}}{\epsilon_\mathbf{p} - \epsilon_\mathbf{q} + i0^+} \right)$$

$$= \frac{i\eta_0\hbar}{m_e} \int \frac{d^3p}{(2\pi)^3} \int \frac{d^3q}{(2\pi)^3} e^{-2a^2|\mathbf{p}-\mathbf{q}|^2} e^{i(\mathbf{q}-\mathbf{p})\cdot\mathbf{r}}$$

$$(\mathbf{p}+\mathbf{q})[\mathbf{L}\cdot(\mathbf{q}\times\mathbf{p})] \frac{f_\mathbf{p} - f_\mathbf{q}}{\epsilon_\mathbf{p} - \epsilon_\mathbf{q} + i0^+}$$

$$= \frac{i\eta_0\hbar}{m_e} \int \frac{d^3p}{(2\pi)^3} \int \frac{d^3q}{(2\pi)^3} e^{-2a^2|\mathbf{p}-\mathbf{q}|^2} e^{i(\mathbf{q}-\mathbf{p})\cdot\mathbf{r}}$$

$$(\mathbf{p}+\mathbf{q})[\mathbf{L}\cdot(\mathbf{q}\times\mathbf{p})] \frac{f_\mathbf{p}}{\epsilon_\mathbf{p} - \epsilon_\mathbf{q} + i0^+} + \text{c.c.}, \quad \text{(A11)}$$

where c.c. stands for the complex conjugate of the other terms.

Using

$$e^{-2a^2|\mathbf{p}-\mathbf{q}|^2} = \frac{\sqrt{2}}{32\pi^{3/2}a^3} \int d^3r' e^{i(\mathbf{q}-\mathbf{p})\cdot\mathbf{r'}} e^{-r'^2/(8a^2)}, \quad \text{(A12)}$$

we can write the regularized velocity, $\langle \mathbf{v}(\mathbf{r}) \rangle$, as the integral of the nonregularized one, $\langle \mathbf{v}_\infty(\mathbf{r}) \rangle$. The latter has a divergence in the origin due to the δ nature of the skew scattering when $a \to 0$, as shown later:

$$\langle \mathbf{v}(\mathbf{r}) \rangle = \frac{\sqrt{2}}{32\pi^{3/2}a^3} \int d^3r' e^{-r'^2/(8a^2)} \langle \mathbf{v}_\infty(\mathbf{r}+\mathbf{r'}) \rangle,$$

$$\langle \mathbf{v}_\infty(\mathbf{r}) \rangle = i\eta_0 \frac{\hbar}{m_e} \int \frac{d^3p}{(2\pi)^3} \int \frac{d^3q}{(2\pi)^3} e^{i(\mathbf{q}-\mathbf{p})\cdot\mathbf{r}}(\mathbf{p}+\mathbf{q})$$

$$\cdot [\mathbf{L}\cdot(\mathbf{q}\times\mathbf{p})] \frac{f_\mathbf{p}}{\epsilon_\mathbf{p} - \epsilon_\mathbf{q} + i0^+} + \text{c.c.} \quad \text{(A13)}$$

The angular part of the integral over $\mathbf{q} = q(\sin\theta_\mathbf{q}\cos\phi_\mathbf{q}\hat{\mathbf{x}} + \sin\theta_\mathbf{q}\sin\phi_\mathbf{q}\hat{\mathbf{y}} + \cos\theta_\mathbf{q}\hat{\mathbf{z}})$ reads

$$I_1 \equiv i \int_0^\pi d\theta_\mathbf{q} \sin\theta_\mathbf{q} \int_0^{2\pi} d\phi_\mathbf{q} e^{i\mathbf{q}\cdot\mathbf{r}}(\mathbf{q}+\mathbf{p})[\mathbf{L}\cdot(\mathbf{q}\times\mathbf{p})]$$

$$= \frac{4\pi i}{qr^3}[qr\cos(qr) - \sin(qr)][\mathbf{L}\times\mathbf{p} + i(\mathbf{r}\cdot\mathbf{J}\times\mathbf{p})\mathbf{p}]$$

$$- \frac{4\pi i}{qr^3}[3qr\cos(qr) - (3-q^2r^2)\sin(qr)](\hat{\mathbf{r}}\cdot\mathbf{L}\times\mathbf{p})\hat{\mathbf{r}}, \quad \text{(A14)}$$

such that the angular integral over $\mathbf{p} = p(\sin\theta_\mathbf{p}\cos\phi_\mathbf{p}\hat{\mathbf{x}} + \sin\theta_\mathbf{p}\sin\phi_\mathbf{p}\hat{\mathbf{y}} + \cos\theta_\mathbf{p}\hat{\mathbf{z}})$ of the previous expression is

$$\int_0^\pi d\theta_\mathbf{p} \sin\theta_\mathbf{p} \int_0^{2\pi} d\phi_\mathbf{p} e^{-i\mathbf{p}\cdot\mathbf{r}}I_1$$

$$= -\frac{32\pi^2}{pqr^5}[pr\cos(pr) - \sin(pr)]$$

$$\times [qr\cos(qr) - \sin(qr)]\mathbf{L}\times\hat{\mathbf{r}}, \quad \text{(A15)}$$

which reveals the rotational (i.e., $\propto \mathbf{L}\times\hat{\mathbf{r}}$) character of the current:

$$\langle \mathbf{v}_\infty \rangle = -\frac{\eta_0}{\pi^4\hbar r^5}\mathbf{L}\times\hat{\mathbf{r}} \int_0^{k_F} dp\, p[pr\cos(pr) - \sin(pr)] \quad \text{(A16)}$$

$$\int_0^\infty dq \frac{q[qr\cos(qr) - \sin(qr)]}{p^2 - q^2 + i0^+} + \text{c.c.} \quad \text{(A17)}$$

Using $\cos(qr) = (e^{iqr} + e^{-iqr})/2$ and $\sin(qr) = (e^{iqr} - e^{-iqr})/(2i)$,

$$\int_0^\infty dq \frac{q[qr\cos(qr) - \sin(qr)]}{p^2 - q^2 + i0^+}$$

$$= -\frac{1}{4} \int_{-\infty}^\infty dq\, q \frac{e^{iqr}(qr+i) + e^{-iqr}(qr-i)}{q^2 - (p+i0^+)^2}, \quad \text{(A18)}$$

the integral over q can be carried out by a contour integral in the complex plane. For $r > 0$ only the poles with a positive (negative) imaginary part contribute for integrands containing e^{iqr} (e^{-iqr}),

$$\int_0^\infty dq \frac{q[qr\cos(qr) - \sin(qr)]}{p^2 - q^2 + i0^+} = -\frac{\pi i}{2}(pr+i)e^{ipr}, \quad \text{(A19)}$$

and

$$\langle \mathbf{v}_\infty \rangle = \frac{\eta_0}{2\pi^3\hbar r^5}\mathbf{L}\times\hat{\mathbf{r}} \int_0^{k_F} dp\, p[pr\cos(pr) - \sin(pr)]$$

$$\times (ipr-1)e^{ipr} + \text{c.c.}$$

$$= -\frac{\eta_0}{\pi^3\hbar r^5}\mathbf{L}\times\hat{\mathbf{r}} \int_0^{k_F} dp\, p[pr\cos(pr) - \sin(pr)]$$

$$[\cos(pr) + pr\sin(pr)]. \quad \text{(A20)}$$

The p integral is straightforward, leading to

$$\langle \mathbf{v}_\infty(\mathbf{r}) \rangle = \frac{\eta_0}{2\pi^3\hbar} \frac{f(r)}{r}\mathbf{L}\times\hat{\mathbf{r}}, \quad \text{(A21)}$$

$$f(x/k_F) = \frac{2x(-9+2x^2)\cos(2x) + (9-14x^2)\sin(2x)}{8(x/k_F)^6}, \quad \text{(A22)}$$

where $x = k_F r$. $f(r)$ oscillates with wave number $2k_F$, as expected for the response of a degenerate electron gas. Moreover, for $r \gg \langle r \rangle$, $f(r) \propto \cos(2k_F r)/r^3$, as well known from the RKKY spin polarization. Finally, the divergence at the origin $\lim_{r\to 0} |\langle \mathbf{v}_\infty(\mathbf{r}) \rangle| = \infty$ comes from δ-function skew-scattering potentials ($a \to 0$) and can be avoided by using Eq. (A13):

$$\langle \mathbf{v}(\mathbf{r}) \rangle = \frac{\eta_0}{2\pi^3\hbar} \frac{F(r)}{r}\mathbf{L}\times\hat{\mathbf{r}}, \quad \text{(A23)}$$

$$F(r) = \frac{1}{ar\sqrt{2\pi}} \int_0^\infty \frac{dr'}{r'} e^{-\frac{r'^2+r^2}{8a^2}}$$
$$\cdot \left[r'r \cosh\left(\frac{r'r}{4a^2}\right) - 4a^2 \sinh\left(\frac{r'r}{4a^2}\right) \right] f(r'). \quad (A24)$$

Both response functions are plotted in Fig. 4.

The angular average of the orbital moment density,

$$\langle \mathbf{l} \rangle(r) \equiv \frac{1}{4\pi} \int_0^{2\pi} d\phi \int_0^\pi d\theta \sin\theta \, m_e \mathbf{r} \times \langle \mathbf{v}(\mathbf{r}) \rangle$$
$$= \frac{m_e \eta_0 F(r)}{3\pi^3 \hbar} \mathbf{L}, \quad (A25)$$

with integrated value

$$\int d^3r \langle \mathbf{l} \rangle(r) = \frac{4m_e \eta_0}{3\pi^2 \hbar} \int_0^\infty dr \, r^2 F(r) \mathbf{L} = G_i^L \mathbf{L},$$

and

$$\int_0^\infty dr \, r^2 F(r) = \int_0^\infty dr \, r^2 f(r) = \frac{k_F^3}{2}. \quad (A26)$$

The above equation states that the integrated orbital moment of both the regularized and the divergent velocity fields are the same,

$$G_i^L = \frac{2m_e \eta_0 k_F^3}{3\pi^2 \hbar} \approx 3.2 \times 10^{-3} \left(\frac{k_F \text{Å}}{1.75}\right)^3, \quad (A27)$$

where in the second step we used η_0 for an Al host metal. The constant G_i^L plays the role of a g factor, and then the rotational current contributes by about 0.3% to the total $4f$ orbital moment.

APPENDIX B: ØRSTED FIELD GENERATED BY THE EQUILIBRIUM CURRENTS

According to Maxwell's equations the equilibrium charge-current vortex around the rare-earth moment generates a magnetic field Eq. (16):

$$\mathbf{B}_\emptyset(\mathbf{R}) = -\frac{e\mu_0}{4\pi} \int d^3r' \langle \mathbf{v}(\mathbf{r}') \rangle \times \frac{\mathbf{R}-\mathbf{r}'}{|\mathbf{R}-\mathbf{r}'|^3}.$$

The derivation of an analytic expression for general $\mathbf{R}$ is tedious. However, far from the RE ion, $R = |\mathbf{R}| \gg \langle r \rangle$, the Taylor expansion of $|R\hat{\mathbf{R}} - \mathbf{r}|^{-3}$ gives

$$\mathbf{B}_\emptyset(\mathbf{R}) = \frac{\mu_0}{4\pi} \frac{3(\mathbf{m_{rc}} \cdot \mathbf{R})\mathbf{R} - R^2 \mathbf{m_{rc}}}{R^5}, \quad (B1)$$

where $\mathbf{m_{rc}} = -\gamma_0 G_i^L \mathbf{L}$. The above expression is the expected result of a field generated by the magnetic moment $\mathbf{m_{rc}}$ of the current vortex.

On the other hand, the magnetic field at the origin $\mathbf{R} = 0$ reads

$$\mathbf{B}_\emptyset(0) = \frac{e\mu_0}{4\pi} \int_0^\infty dr \int_0^\pi d\theta \sin\theta \int_0^{2\pi} d\phi \langle \mathbf{v}(\mathbf{r}) \rangle \times \hat{\mathbf{r}},$$
$$= \frac{\eta_0}{2\pi^3 \hbar} \frac{e\mu_0}{4\pi} \int_0^\infty dr \frac{F(r)}{r} \int_0^\pi d\theta \sin\theta$$
$$\times \int_0^{2\pi} d\phi (\mathbf{L} \times \hat{\mathbf{r}}) \times \hat{\mathbf{r}}$$

$$= -3.5 \times 10^{-7} \frac{e\eta_0 \mu_0}{\hbar a^6} \mathbf{L}. \quad (B2)$$

APPENDIX C: ORBITAL ANGULAR MOMENTUM DENSITY IN SECOND QUANTIZATION

The Pauli equation for an electron wave function $\boldsymbol{\psi}(\mathbf{r})$ with energy E in a homogeneous magnetic field $\mathbf{B}$ reads

$$E\boldsymbol{\psi}(\mathbf{r}) = \left[\frac{1}{2m_e}(-i\hbar\nabla + e\mathbf{A})^2 + \frac{e\hbar}{2m_e}\boldsymbol{\sigma} \cdot \mathbf{B} \right] \boldsymbol{\psi}(\mathbf{r}). \quad (C1)$$

In the symmetric gauge $\mathbf{A} = \frac{1}{2}\mathbf{B} \times \mathbf{r}$,

$$E = \int d^3r \boldsymbol{\psi}^\dagger(\mathbf{r}) \left[\frac{1}{2m_e}\left(-i\hbar\nabla + \frac{e}{2}\mathbf{B} \times \mathbf{r}\right)^2 + \frac{e\hbar}{2m_e}\boldsymbol{\sigma} \cdot \mathbf{B} \right] \boldsymbol{\psi}(\mathbf{r})$$
$$= \int d^3r \boldsymbol{\psi}^\dagger(\mathbf{r}) \left[-\frac{\hbar^2\nabla^2}{2m_e} - ie\hbar\frac{(\mathbf{B} \times \mathbf{r}) \cdot \nabla + \nabla \cdot (\mathbf{B} \times \mathbf{r})}{4m_e} \right.$$
$$\left. + \frac{e\hbar}{2m_e}\boldsymbol{\sigma} \cdot \mathbf{B} + \mathcal{O}(B^2) \right] \boldsymbol{\psi}(\mathbf{r}). \quad (C2)$$

Then the energy of the Zeeman coupling E_Z is

$$E_Z = \frac{e}{2m_e}(\mathbf{l}_T + 2\mathbf{s}_T) \cdot \mathbf{B}, \quad (C3)$$

where the factor 2 is the single-electron orbital g factor. In terms of the total spin $\mathbf{s}_T$ and orbital $\mathbf{l}_T$ angular momenta,

$$\mathbf{s}_T = \frac{\hbar}{2} \int d^3r \boldsymbol{\psi}^\dagger(\mathbf{r})\boldsymbol{\sigma}\boldsymbol{\psi}(\mathbf{r}), \quad (C4)$$

$$\mathbf{l}_T = \frac{i\hbar}{2} \int d^3r \boldsymbol{\psi}^\dagger(\mathbf{r})(\nabla \times \mathbf{r} - \mathbf{r} \times \nabla)\boldsymbol{\psi}(\mathbf{r}). \quad (C5)$$

Substituting

$$\boldsymbol{\psi}(\mathbf{r}) = \frac{1}{\sqrt{\Omega}} \sum_{\mathbf{p},\alpha} e^{i\mathbf{p}\cdot\mathbf{r}} \chi_\alpha a_{\mathbf{p}\alpha}, \quad (C6)$$

$$\boldsymbol{\psi}^\dagger(\mathbf{r}) = \frac{1}{\sqrt{\Omega}} \sum_{\mathbf{q},\beta} e^{-i\mathbf{q}\cdot\mathbf{r}} \chi_\beta^\dagger a_{\mathbf{q}\beta}^\dagger, \quad (C7)$$

where the spinors $\chi_\uparrow$ and $\chi_\downarrow$ are the basis of σ_z. The second quantized version of $\mathbf{s}(\mathbf{r})$ and $\mathbf{l}(\mathbf{r})$, the local densities of spin and orbital momentum (relative to the origin), respectively:

$$\mathbf{s}_T = \int \mathbf{s}(\mathbf{r})d^3r, \quad (C8)$$

$$\mathbf{s}(\mathbf{r}) = \frac{\hbar}{2} \frac{1}{\Omega} \sum_{\mathbf{p}\mathbf{q}\alpha\beta} e^{i(\mathbf{p}-\mathbf{q})\cdot\mathbf{r}} a_{\mathbf{q}\beta}^\dagger \boldsymbol{\sigma}_{\alpha\beta} a_{\mathbf{p}\alpha}, \quad (C9)$$

and

$$\mathbf{l}_T = \frac{i\hbar}{2} \int d^3r \boldsymbol{\psi}^\dagger(\mathbf{r})(\nabla \times \mathbf{r} - \mathbf{r} \times \nabla)\boldsymbol{\psi}(\mathbf{r}) = \int \mathbf{l}(\mathbf{r})d^3r, \quad (C10)$$

with

$$\mathbf{l}(\mathbf{r}) = \frac{\hbar}{\Omega}\mathbf{r} \times \sum_{\mathbf{p}\mathbf{q}\gamma} e^{i(\mathbf{p}-\mathbf{q})\cdot\mathbf{r}} \mathbf{p} a_{\mathbf{q}\gamma}^\dagger a_{\mathbf{p}\gamma}$$
$$= \frac{\hbar}{\Omega}\mathbf{r} \times \sum_{\mathbf{p}\mathbf{q}\gamma} e^{i(\mathbf{p}-\mathbf{q})\cdot\mathbf{r}} \frac{\mathbf{p}+\mathbf{q}}{2} a_{\mathbf{q}\gamma}^\dagger a_{\mathbf{p}\gamma}. \quad (C11)$$

Note that $\mathbf{l}_T = m_e \mathbf{r}_{op} \times \mathbf{v}_{op}$, where $\mathbf{r}_{op}$ and $\mathbf{v}_{op}$ are the position and velocity operators, respectively.

[1] Y. Otani, M. Shiraishi, A. Oiwa, E. Saitoh, and S. Murakami, Spin conversion on the nanoscale, Nat. Phys. **13**, 829 (2017).

[2] K. Garello, I. M. Miron, C. O. Avci, F. Freimuth, Y. Mokrousov, S. Blügel, S. Auffret, O. Boulle, G. Gaudin, and P. Gambardella, Symmetry and magnitude of spin-orbit torques in ferromagnetic heterostructures, Nat. Nano. **8**, 587 (2013).

[3] K. Nomura and D. Kurebayashi, Charge-Induced Spin Torque in Anomalous Hall Ferromagnets, Phys. Rev. Lett. **115**, 127201 (2015).

[4] C. Ciccarelli, K. M. D. Hals, A. Irvine, V. Novak, Y. Tserkovnyak, H. Kurebayashi, A. Brataas, and A. Ferguson, Magnonic charge pumping via spin-orbit coupling, Nat. Nano. **10**, 50 (2015).

[5] M. Mori, A. Spencer-Smith, O. P. Sushkov, and S. Maekawa, Origin of the Phonon Hall Effect in Rare-Earth Garnets, Phys. Rev. Lett. **113**, 265901 (2014).

[6] A. M. Kadomtseva, Y. F. Popov, G. P. Vorob'ev, N. V. Kostyuchenko, A. I. Popov, A. A. Mukhin, V. Yu. Ivanov, L. N. Bezmaternykh, I. A. Gudim, V. L. Temerov, A. P. Pyatakov, and A. K. Zvezdin, High-temperature magnetoelectricity of terbium aluminum borate: The role of excited states of the rare-earth ion, Phys. Rev. B **89**, 014418 (2014).

[7] A. I. Popov, D. I. Plokhov, and A. K. Zvezdin, Anapole moment and spin-electric interactions in rare-earth nanoclusters, Euro. Phys. Lett. **87**, 67004 (2009).

[8] A. O. Leon, A. B. Cahaya, and G. E. W. Bauer, Voltage Control of Rare-Earth Magnetic Moments at the Magnetic-Insulator−Metal Interface, Phys. Rev. Lett. **120**, 027201 (2018).

[9] A. A. Baker, A. I. Figueroa, G. van der Laan, and T. Hesjedal, Tailoring of magnetic properties of ultrathin epitaxial Fe films by Dy doping, AIP Adv. **5**, 077117 (2015).

[10] W. Zhang, D. Zhang, P. K. J. Wong, H. Yuan, S. Jiang, G. van der Laan, Y. Zhai, and Z. Lu, Selective tuning of Gilbert damping in spin-valve trilayer by insertion of rare earth nanolayers, ACS Appl. Mater. Interfaces **7**, 17070 (2015).

[11] Y. Sun, Y-Y. Song, H. Chang, M. Kabatek, M. Jantz, W. Schneider, M. Wu, H. Schultheiss, and A. Hoffmann, Growth and ferromagnetic resonance properties of nanometer-thick yttrium iron garnet films, Appl. Phys. Lett. **101**, 152405 (2012).

[12] G. F. Dionne, *Magnetic Oxides* (Springer, London, 2009).

[13] A. J. Moulson and J. M. Herbert, *Electroceramics: Materials, Properties, Applications* (Wiley, New York, 2003).

[14] E. R. Rosenberg, L. Beran, C. O. Avci, C. Zeledon, B. Song, C. Gonzalez-Fuentes, J. Mendil, P. Gambardella, M. Veis, C. Garcia, G. S. D. Beach, and C. A. Ross, Magnetism and spin transport in rare-earth-rich epitaxial terbium and europium iron garnet films, Phys. Rev. Materials **2**, 094405 (2018).

[15] M. Imai, H. Chudo, M. Ono, K. Harii, M. Matsuo, Y. Ohnuma, S. Maekawa, and E. Saitoh, Angular momentum compensation manipulation to room temperature of the ferrimagnet $Ho_{3-x}Dy_xFe_5O_{12}$ detected by the Barnett effect, Appl. Phys. Lett. **114**, 162402 (2019).

[16] S. Geprägs, A. Kehlberger, F. D. Coletta, Z. Qiu, E-J. Guo, T. Schulz, C. Mix, S. Meyer, A. Kamra, M. Althammer, H. Huebl, G. Jakob, Y. Ohnuma, H. Adachi, J. Barker, S. Maekawa, G. E. W. Bauer, E. Saitoh, R. Gross, S. T. B. Goennenwein, and M. Klaüi, Origin of the spin Seebeck effect in compensated ferrimagnets, Nat. Commun. **7**, 10452 (2016).

[17] M. Kubota, A. Tsukazaki, F. Kagawa, K. Shibuya, Y. Tokunaga, M. Kawasaki, and Y. Tokura, Stress-induced perpendicular magnetization in epitaxial iron garnet thin films, APEX **5**, 103002 (2012).

[18] C. Tang, P. Sellappan, Y. Liu, Y. Xu, J. E. Garay, and J. Shi, Anomalous Hall hysteresis in Tm3Fe5O12/Pt with strain-induced perpendicular magnetic anisotropy, Phys. Rev. B **94**, 140403(R) (2016).

[19] C. N. Wu, C. C. Tseng, Y. T. Fanchiang, C. K. Cheng, K. Y. Lin, S. L. Yeh, S. R. Yang, C. T. Wu, T. Liu, M. Wu, M. Hong, and J. Kwo, High-quality thulium iron garnet films with tunable perpendicular magnetic anisotropy by off-axis sputtering-correlation between magnetic properties and film strain, Sci. Rep. **8**, 11087 (2018).

[20] C. O. Avci, A. Quindeau, C.-F. Pai, M. Mann, L. Caretta, A. S. Tang, M. C. Onbasli, C. A. Ross, and G. S. D. Beach, Current-induced switching in a magnetic insulator, Nat. Mater. **16**, 309 (2017).

[21] C. O. Avci, A. Quindeau, M. Mann, C-F. Pai, C. A. Ross, and G. S. D. Beach, Spin transport in as-grown and annealed thulium iron garnet/platinum bilayers with perpendicular magnetic anisotropy, Phys. Rev. B **95**, 115428 (2017).

[22] A. Quindeau, C. O. Avci, W. Liu, C. Sun, M. Mann, A. S. Tang, M. C. Onbasli, D. Bono, P. M. Voyles, Y. Xu, J. Robinson, G. S. D. Beach, and C. A. Ross, Tm3Fe5O12/Pt heterostructures with perpendicular magnetic anisotropy for spintronic applications, Adv. Electron. Mater. **3**, 1600376 (2017).

[23] J. Jensen and A. R. Mackintosh, *Rare Earth Magnetism* (Clarendon Press, Oxford, 1991).

[24] A. Fert and A. Friederich, Skew scattering by rare-earth impurities in silver, gold, and aluminum, Phys. Rev. B **13**, 397 (1976).

[25] E. Belorizki, J. J. Niez, and P. M. Levy, Orbital and spin polarization of conduction electrons in rare-earth intermetallic compounds. Theory, Phys. Rev. B **23**, 3360 (1981).

[26] B. Barbara, M. F. Rossignol, E. Belorizky, and P. M. Levy, Orbital exchange in the rare-earth dialuminides, Solid State Commun. **46**, 669 (1983).

[27] R. Devine, d Resonance effects associated with rare earths and dilute rare earth alloys, J. Phys. F: Met. Phys. **4**, 1447 (1974).

[28] K. Jiang, X. Dai, and Z. Wang, Quantum Anomalous Vortex and Majorana Zero Mode in Iron-Based Superconductor Fe(Te, Se), Phys. Rev. X **9**, 011033 (2019).

[29] J. Kondo, Anomalous Hall effect and magnetoresistance of ferromagnetic metals, Prog. Theor. Phys. **27**, 772 (1962).

[30] M. A. Ruderman and C. Kittel, Indirect exchange coupling of nuclear magnetic moments by conduction electrons, Phys. Rev. **96**, 99 (1954); T. Kasuya, A theory of metallic ferro- and antiferromagnetism on Zener's model, Progr. Theoret. Phys. **16**, 45 (1956); K. Yosida, Magnetic properties of Cu-Mn alloys, Phys. Rev. **106**, 893 (1957).

[31] S. H. Liu, Exchange interaction between conduction electrons and magnetic shell electrons in rare-earth metals, Phys. Rev. **121**, 451 (1961).

[32] K. Oyanagi, S. Takahashi, L. J. Cornelissen, J. Shan, S. Daimon, T. Kikkawa, G. E. W. Bauer, B. J. van Wees, and E. Saitoh, Spin transport in insulators without exchange stiffness, Nat. Commun. **10**, 4740 (2019).

[33] J. Sievers, Asphericity of 4f-shells in their Hund's rule ground states, Z. Phys. B: Condens. Matter **45**, 289 (1982).

[34] R. Brout and H. Suhl, Effects of Spin-Orbit Coupling in Rare Earth Metals, And in Solutions of Rare Earth Metals, Phys. Rev. Lett. **2**, 387 (1959).

[35] H. P. Van der Braak and W. J. Caspers, s-f Scattering in rare-earth metals, Phys. Lett. **16**, 212 (1965).

[36] B. Giovannini, Theory of the anomalous Hall effect in the rare earths, Phys. Lett. A **36**, 381 (1971).

[37] R. G. Barnes and E. D. Jones, Strength of the s-f exchange interaction in rare-earth intermetallics, Solid State Commun. **5**, 285 (1967).

[38] C. Rettori, D. Davidov, R. Orbach, E. P. Chock, and B. Ricks, Electron-spin resonance of rare earths in aluminum, Phys. Rev. B **7**, 1 (1973).

[39] B. Giovannini, Skew scattering in dilute alloys. I. The Kondo model, J. Low Temp. Phys. **11**, 489 (1973).

[40] A. Fert, Transport in magnetic alloys: Scattering asymmetries (anisotropic scattering, skew scattering, side-jump), Physica **86**, 491 (1977).

[41] A. Fert and P. M. Levy, Magnetotransport properties of noble metals containing rare-earth impurities. II. Theory, Phys. Rev. B **16**, 5052 (1977).

[42] G. Lacueva, P. M. Levy, and A. Fert, Unified approach to some transport and EPR properties of noble metals with rare-earth impurities, Phys. Rev. B **26**, 1099 (1982).

[43] D. Eagles, Models for the heavy rare earth metals and (rare earth) Fe 2 compounds involving 5 d and 6 s electrons, Phys. kondens. Mater. **16**, 181 (1973).

[44] J. M. Dixon, 5d and 4f mixing coefficients for rare earth ions in the pure metals and in silver and gold, Solid State Commun. **12**, 789 (1973).

[45] R. A. B. Devine, A. Ludwig, J. M. Dixon, Localisation of 5d electrons in rare-earth metals, Phys. Lett. A **45**, 249 (1973).

[46] B. Zygmunt and W. Gruhn, Virtual bound state contribution to the magnetic moment of an ion in a multilayered system, J. Alloys Compd. **219**, 296 (1995).

[47] A. B. Cahaya, A. O. Leon, and G. E. W. Bauer, Crystal field effects on spin pumping, Phys. Rev. B **96**, 144434 (2017).

[48] A. Cottet and W. Belzig, Superconducting proximity effect in a diffusive ferromagnet with spin-active interfaces, Phys. Rev. B **72**, 180503(R) (2005).

[49] C. Kittel, *Introduction to Solid State Physics* (Wiley, New York, 2005).

[50] D. M. Nisson and N. J. Curro, Nuclear magnetic resonance Knight shifts in the presence of strong spin orbit and crystal-field potentials, New J. Phys. **18**, 073041 (2016).

[51] C. Granata and A. Vettoliere, Nano superconducting quantum interference device: A powerful tool for nanoscale investigations, Phys. Rep. **614**, 1 (2016).

[52] R. Schirhagl, K. Chang, M. Loretz, and C. L. Degen, Nitrogen-vacancy centers in diamond: Nanoscale sensors for physics and biology, Annu. Rev. Phys. Chem. **65**, 83 (2014).

[53] F. Casola, T. van der Sar, and A. Yacoby, Probing condensed matter physics with magnetometry based on nitrogen-vacancy centres in diamond, Nat. Rev. Mater. **3**, 17088 (2018).